JACS
JOURNAL OF THE AMERICAN CHEMICAL SOCIETY
pubs.acs.org/JACS
Article

Addition Reaction between Piperidine and C_{60} to Form 1,4-Disubstituted C_{60} Proceeds through van der Waals and Dative Bond Complexes: Theoretical and Experimental Study

Rabindranath Lo,[‖] Debashree Manna,[‖] Maximilián Lamanec,[‖] Weizhou Wang, Aristides Bakandritsos, Martin Dračínský, Radek Zbořil, Dana Nachtigallová,* and Pavel Hobza*

Cite This: *J. Am. Chem. Soc.* 2021, 143, 10930−10939

ABSTRACT: A combined computational and experimental study reveals the character of the C_{60} complexes with piperidine formed under different reaction conditions. The IR and NMR experiments detect the dative bond complex, which according to NMR, is stable in the oxygen-free environment and transforms to the adduct complex in the presence of O_2. Computational studies on the character of reaction channels rationalize the experimental observations. They show that the piperidine dimer rather than a single piperidine molecule is required for the complex formation. The calculations reveal significant differences in the dative bond and adduct complexes' character, suggesting a considerable versatility in their electronic properties modulated by the environment. This capability offers new application potential in several fields, such as in energy storage devices.

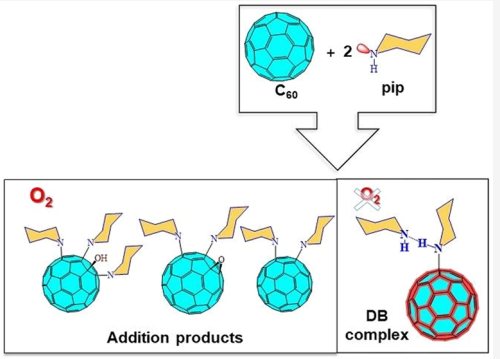

1. INTRODUCTION

The amino-functionalization of carbon nanomaterials undoubtedly represents one of the most popular modifications providing promising systems with applications in several fields.[1] The uses of amino-fullerenes in biorelated disciplines,[2−9] optoelectronics,[10−13] and catalysis[14−16] have already been reported, although there are still many to be uncovered.

The unique structure of fullerenes gives these carbon allotropes the capability to modify their electronic properties widely. This flexibility, among others, makes fullerenes promising candidates for, e.g., battery applications (for review, see ref 17). In this context, the properties of functionalized C_{60}, such as tuning of their redox potentials, directly related to the electron affinity, and others, have been the subjects of several studies[18−20] for their potential use as electrode materials in batteries.[17] As an example, the fullerene's functionalization can change its overall charge, ranging from negative carboxyl-C_{60} to neutral ester-C_{60} and positive piperazine-C_{60}.[21]

The addition of amines to C_{60} fullerene was first reported nearly three decades ago.[22,23] The resulting products were identified as tetraaminofullerene epoxides with a 1,4-addition pattern.[24−26] The observed reaction yield turned out to be very low; however, it increased upon the UV irradiation.[27,28] Lately, penta-amino hydroxyl and hexa-amino adducts have also been synthesized in dark conditions.[29]

It is now generally assumed that the addition starts with the formation of a long-lived contact ion pair (IP; $[C_{60}^{\bullet-}NHR_2^{\bullet+}]$) resulting from the single-electron transfer (SET) from amine to C_{60}. The SET has been experimentally identified using the near-infrared (NIR) spectroscopy for some tertiary amines-to-fullerene additions[30−32] and secondary amines-to-fullerene additions in polar solvents.[33] The SET process in the amines-to-fullerene addition has also been detected in the reaction of amines and C_{60}/C_{70} fullerenes performed under UV irradiation (photoinduced electron transfer).[34,35]

Detailed studies on the mechanism of the addition reaction of piperidine and other secondary aliphatic amines with C_{60} have shown a substantial increase of the reaction yield of the addition reaction in the polar dimethyl sulfoxide (DMSO)/chlorobenzene solvent mixture,[33] highlighting a crucial role of DMSO to form an IP and subsequent adduct (1,4-tetraaminofullerene epoxide) upon contact with air. Notably, the $C_{60}^{\bullet-}$ characteristic NIR bands (994 and 1077 nm) have not been observed for other mixtures than those containing DMSO.

The above-observed experimental findings, particularly the role of DMSO together with the lack or a lower extent of IP

Received: February 8, 2021
Published: July 16, 2021

https://doi.org/10.1021/jacs.1c01542
J. Am. Chem. Soc. 2021, 143, 10930−10939

Scheme 1. Schematic Diagram Illustrating the Formation of the Addition Products from C_{60} with Piperidine

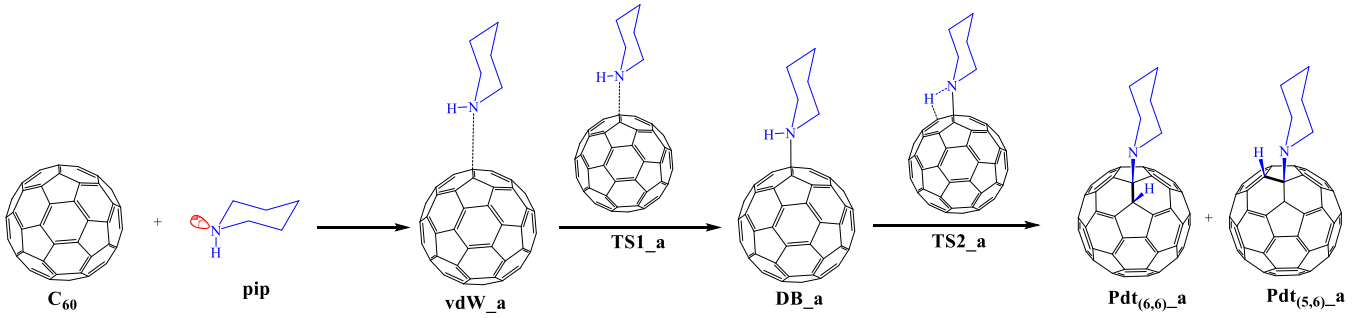

Scheme 2. Schematic Diagram Illustrating the Formation of the Addition Products from C_{60} with Piperidine Dimer

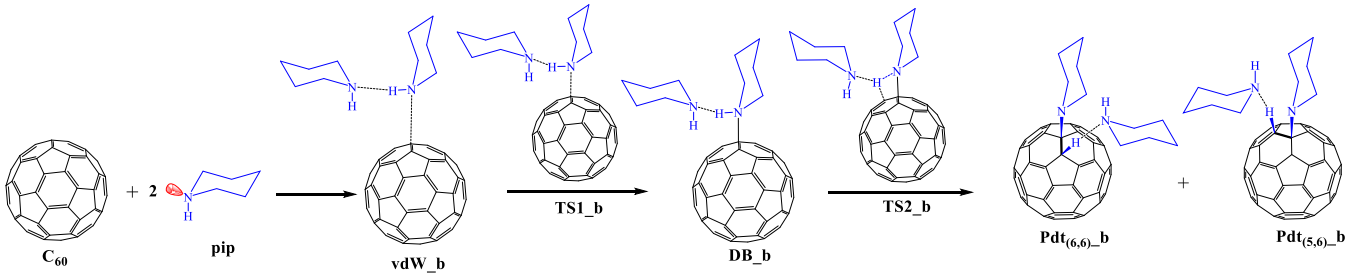

formation,[33] leave the question of the addition mechanism in less polar or nonpolar solvents still open.

We have recently reported on the formation of covalent/dative bonds between C_{60} and piperidine in the less polar solvents, proved by the NMR and IR spectroscopy performed in *o*-dichlorobenzene and pure piperidine, respectively, in which the nitrogen lone pair of piperidine donates two electrons to electron acceptor C_{60}.[36] Using the computational studies, we have shown that this reaction requires hydrogen-bonded piperidine dimer binding, promoting the charge transfer cascade in the sequence *outer* pip → *inner* pip → C_{60}. The existence of the dative complex has been confirmed by IR and NMR experiments. The dative bond (DB) forms practically immediately after putting the reactants together.

The unique properties of fullerene-based materials make it attractive to search for other possible differences in electronic properties due to differences in their bonding characters, such as in their DB and adduct complexes. For this reason, we extend our studies to more detailed calculations of the reaction of C_{60} with piperidine with calculations of the relevant reaction channels of C_{60}···pip and C_{60}···$(pip)_2$ complex formations under an oxygen-free atmosphere (Schemes 1 and 2, respectively) and in the presence of oxygen (Scheme 3 and 4, respectively). The reaction path in Scheme 3 follows that suggested in refs 29 and 33. Contrary to our previous papers dealing exclusively with the DB formation, we also consider the consecutive addition reaction to form 1,4-substituted fullerenes. Previous DFT studies[37−39] show that the addition of amines most likely proceeds across the (6,6) bonds of C_{60} rather than the (5,6) bonds (Figure S1). Our study considers both possible adducts formed from the DB complex. The electronic properties, in particular, charge distribution and electron affinities, for both types of complexes are discussed. The calculations are combined with IR and NMR experiments, run in dark and light and with or without air, allowing the discussion of complex stabilities under different conditions. The experiments are performed in solvents significantly less polar than DMSO (cf. D_e(DMSO) = 46.7 and D_e(CS_2) = 2.6 used in the IR experiment and D_e(*o*-dichloro-benzene) = 9.9 used in the NMR experiment).

2. RESULTS AND DISCUSSION

2.1. Calculations. *2.1.1. C_{60}···pip and C_{60}···$(pip)_2$.* Figures 1 and S2 show the potential energy surface (PES) of forming the C_{60}−pip complex in the absence of oxygen (Scheme 1) and the most important geometry parameters of the PES's critical points. During the reaction course in the gas phase, piperidine binds to C_{60} via a tetrel bond, leading to the van der Waals (vdW) complex (vdW_a), stabilized by 6.7 kcal/mol. The N−H bond of piperidine changes only negligibly. The reaction then proceeds via transition state TS1_a to the DB_a complex. In the former, the piperidine N−H bond remains unchanged, and the C−N bond between C_{60} and piperidine shortens by about 0.9 Å. The reaction barrier is tiny, and the transition states are stable with respect to their isolated subsystems by 1.7 kcal/mol, which makes the DB_a complex easily accessible. The optimization procedure reveals only small changes in the complex, particularly, shortening of the C−N bond by about 0.2 Å and a slight deformation of the C_{60} buckyball structure due to a partial sp^3 hybridization of the carbon atom involved in the dative bond. The stabilization energies of vdW_a and DB_a reveal the former's larger thermodynamic stability, which indicates that the existence of the DB_a complex is unlikely. This picture changes when the solvent is involved in the calculations. Although the calculations localized the vdW_a complex on the PES, this will not form in the solvent, and the reaction will follow directly to the DB_a complex. Most importantly, the DB_a complex's stabilization is significantly larger than in the gas phase (by about 7 kcal/mol), which results during the N → C dative bond formation in the presence of the piperidine solvent.

Starting at the DB_a complex, the reaction profiles are very similar in the gas phase and solvent and are discussed simultaneously. On the basis of the previous experimental and

https://doi.org/10.1021/jacs.1c01542
J. Am. Chem. Soc. 2021, 143, 10930−10939

Scheme 3. Schematic Diagram Illustrating the Formation of the Addition Products from C_{60} with Piperidine in the Presence of O_2

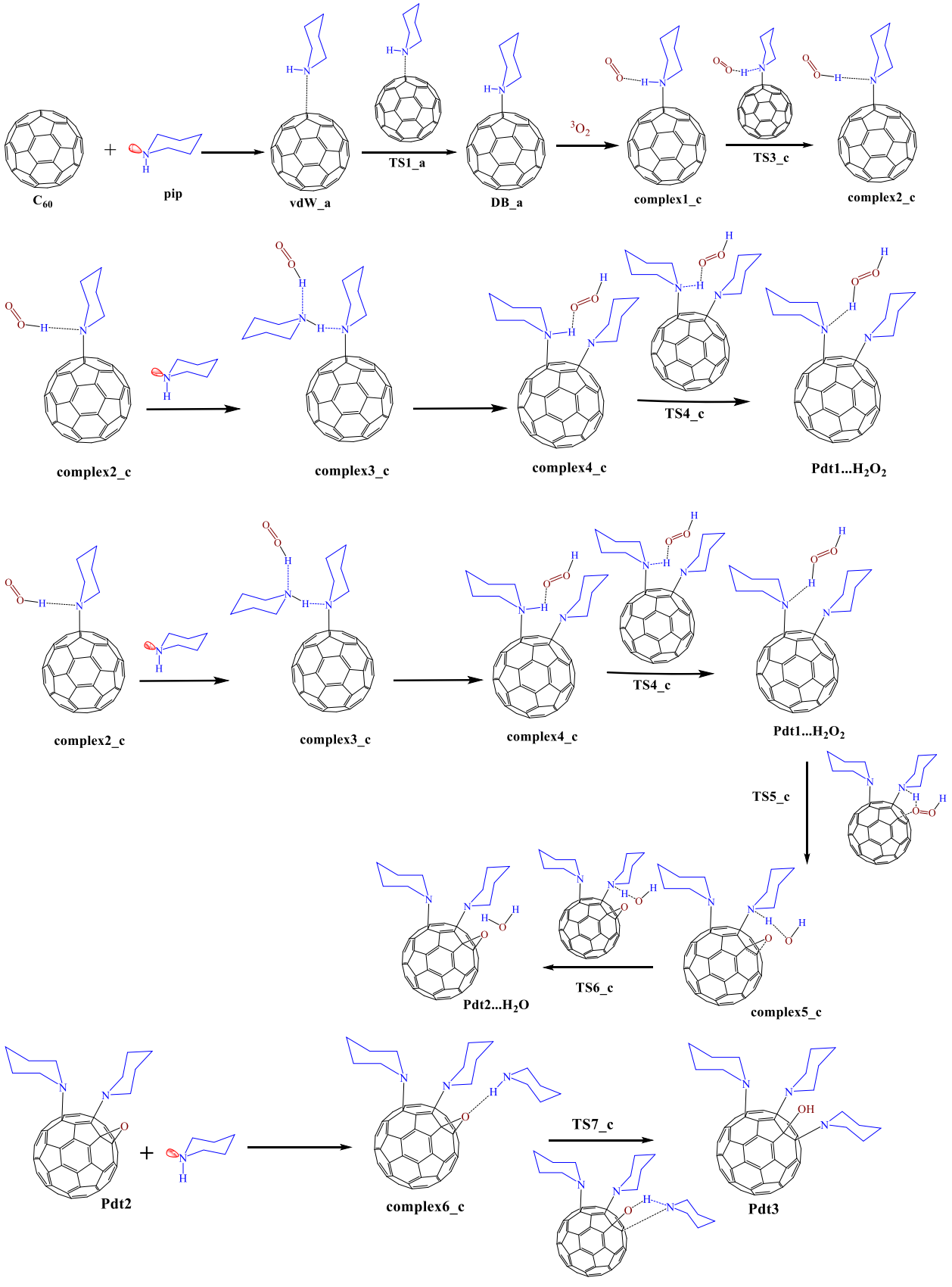

computational findings,[36] two adducts, $Pdt_{(5,6)}$_a and $Pdt_{(6,6)}$_a, and their relevant transitions states, $TS2_{(5,6)}$_a and $TS2_{(6,6)}$_a, were considered. In both cases, the hydrogen of piperidine binds to the C_{60} skeleton. Simultaneously, the

https://doi.org/10.1021/jacs.1c01542
J. Am. Chem. Soc. 2021, 143, 10930−10939

Scheme 4. Schematic Diagram Illustrating the Formation of the Addition Products from C_{60} with Piperidine Dimer in the Presence of O_2

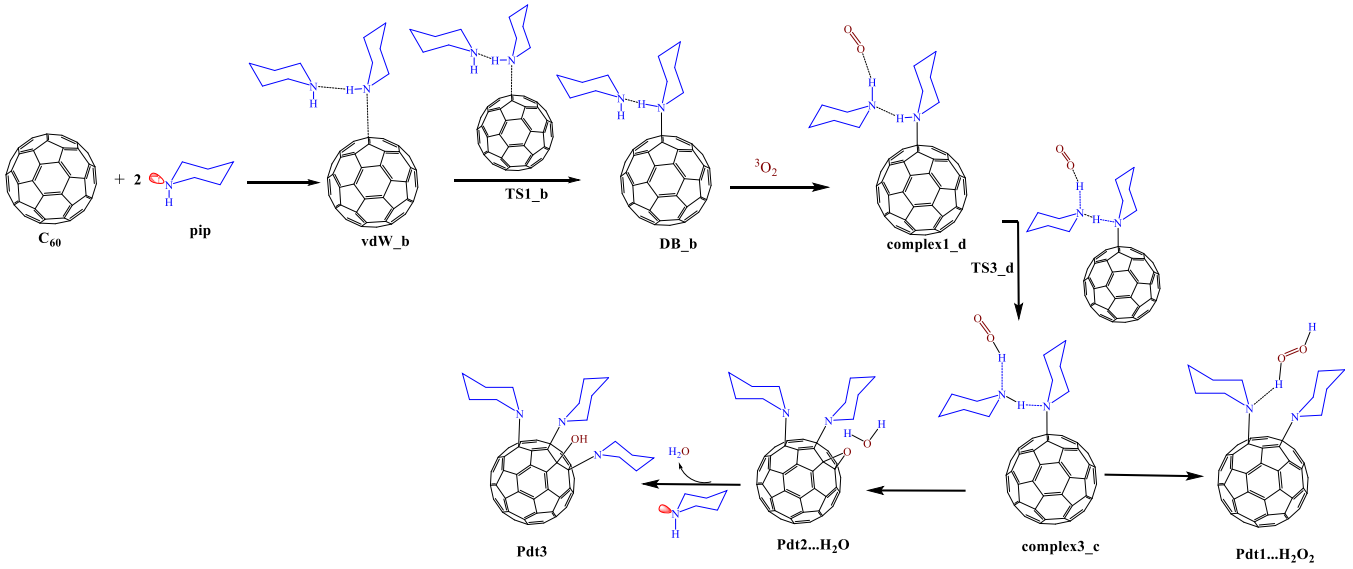

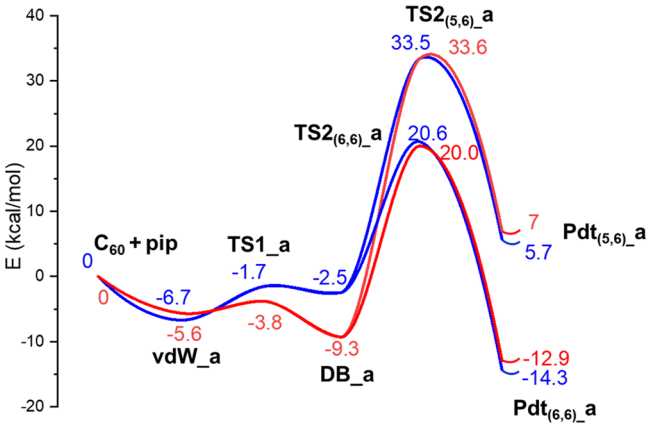

Figure 1. Electronic energy diagram for forming the addition product from C_{60} with piperidine in the gas phase (blue color) and pip solvent (red color).

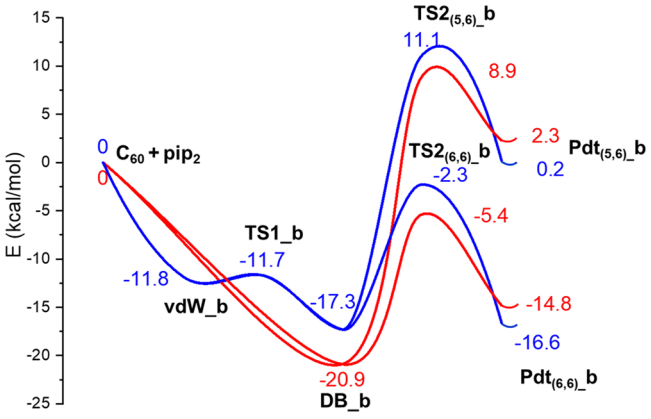

Figure 2. Electronic energy diagram for forming the addition product from C_{60} with piperidine dimer in the gas phase (blue color) and pip solvent (red color).

covalent N−H piperidine bond of about 1.02 Å changes to a noncovalent hydrogen bond of 2.3−2.4 Å. The values of stabilization and activation energies in both the gas and solvent exclude the existence of the complexes with (5,6) binding mode. $Pdt_{(6,6)}$_a corresponds to the most thermodynamically stable structure on the PESs. However, the transition barrier of about 20 kcal/mol calculated for DB_a → $Pdt_{(6,6)}$_a reaction excludes the existence of the latter.

The extension of the system to C_{60}−$(pip)_2$ (Scheme 2) leads to significant modifications in the reaction profile (see Figure 2). The vdW complex (vdW_b) forms only in the gas phase. Its stability is larger, about 12 kcal/mol, compared to C_{60}−pip (7 kcal/mol). Figure S3 shows the most relevant geometry parameters, i.e., the C−N distance between the piperidine directly bound to C_{60} (*inner* pip) and the hydrogen bond between the *inner* and the second (*outer* pip) molecules. From the vdW_b complex, the system reaches the DB_b complex via the TS1_b transition state with a negligible activation barrier of 0.1 kcal/mol.

The calculations performed in the solvent localized neither vdW_b nor TS1_b structures; instead, the optimization led directly to the DB_b complex. This result can be explained by a different charge distribution in pip_2 in the gas and solvent phase (Figure S4). The molecular electrostatic potential (MESP) isosurface exhibits a more negative ESP at the N atom in pip_2 in the solvent medium (−46.8 and −52.7 kcal/mol in the gas and solvent phase, respectively). The DB_b complex possesses one dative bond between C_{60} and pip dimer, instead of the DB_b′ complex having two direct bonds (Figure S5). The former complex is stabilized by (i) the N → C dative bond with the bond length of about 1.57 Å and (ii) the *inner* pip···*outer* pip hydrogen bond of about 1.75 Å, leading to the overall stabilization energies of 17.3 and 20.9 kcal/mol in the gas phase and solvent, respectively. The latter value is in good agreement with the result (18.0 kcal/mol) obtained with a more accurate SCS-MP2 method. Due to similar energy reasons as in the case of C_{60}···pip, only the reaction channel leading to $Pdt_{(6,6)}$_b is discussed next. In this product, the *inner* pip···*outer* pip hydrogen bond breaks, and the hydrogen atom of the former binds to C_{60} and forms a new hydrogen bond, of about 2.2 Å, with the *outer* pip. The $Pdt_{(6,6)}$_b complex stability is 16.6 and 14.8 kcal/mol in the gas

https://doi.org/10.1021/jacs.1c01542
J. Am. Chem. Soc. 2021, 143, 10930−10939

phase and solvent, respectively. The SCS-MP2 stabilization energy in the solvent of 13.0 kcal/mol agrees with the latter DFT-D value. Although this complex stability is only about 2 kcal/mol larger than for C_{60}···pip, its formation is much more likely since the activation reaction for the DB_b → $Pdt_{(6,6)}$_b reaction is energetically feasible; i.e., the $TS2_{(6,6)}$_b transition state is stable by 2.3 kcal/mol (the gas phase) and 5.4 kcal/mol (the solvent) with respect to the reactants. However, their relative stabilities indicate that the former is thermodynamically favored. Indeed, the equilibrium between them shifts toward the DB_b complex (K = 0.00003, ΔG is approximated by ΔE), thus disfavoring $Pdt_{(6,6)}$_b formation.

2.1.2. C_{60}···pip and C_{60}···$(pip)_2$ in the Presence of O_2. Scheme 3 displays the whole reaction scenario leading to three possible reaction products, Pdt1, Pdt2, and Pdt3, starting with a single pip, referred to in the literature (see refs 29 and 33); Scheme 4 illustrates the modifications caused by the interaction with $(pip)_2$. In the reaction path calculations of both C_{60}···pip (see Figure 3 for PES and Figure S6 for the

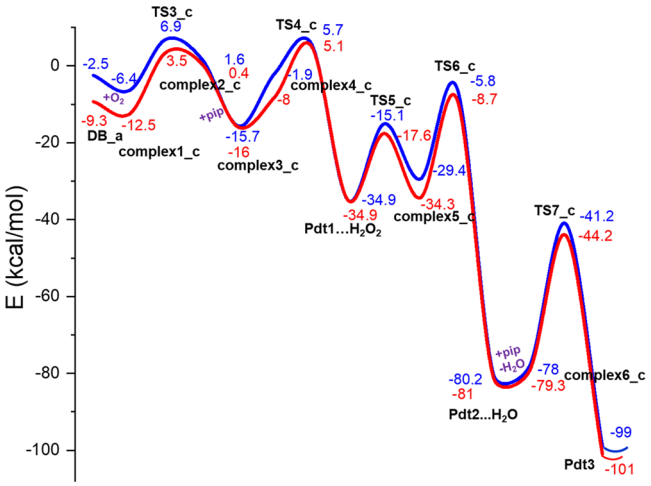

Figure 3. Electronic energy diagram for forming the addition product from C_{60} with pip in the presence of O_2 in the gas phase (blue color) and pip solvent (red color).

structures) and C_{60}···$(pip)_2$ (see Figure 4 for PES and Figure S7 for the structures), the DB complexes (DB_a and DB_b) are considered the starting points for subsequent reactions with O_2. Starting from the C_{60}···pip DB_a complex, O_2 binds via an O···H−N hydrogen bond to piperidine, forming the complex1_c, stabilized by 6.4 and 12.5 kcal/mol in the gas phase and solvent, respectively. At this point, the hydrogen atom from pip transfers to $^3O_2$ and forms hydroperoxyl radical, which interacts with the nitrogen of piperidine via an N−H hydrogen bond of about 1.6 Å (complex2_c). This reaction proceeds on the triplet potential energy surface. The transition barrier (transition state TS3_c) for this reaction is 6.9 and 3.5 kcal/mol in the gas phase and solvent, respectively, and the complex2_c is slightly unstable, by 1.6 and 0.4 kcal/mol in the gas phase and solvent, respectively. The spin density plots of complex2_c and complex3_c show the distribution of spin in C_{60} and the hydroperoxyl radical (Figure S8). The role of C_{60} in the H transfer is apparent from the energy barriers calculated in the absence of C_{60} and presence of O_2 (Figures S9−S12). The corresponding transition barriers for pip (Figures 3 and S10) and pip dimer (Figures 4 and S12) become smaller in the presence of C_{60}. The binding of $^3O_2$ to

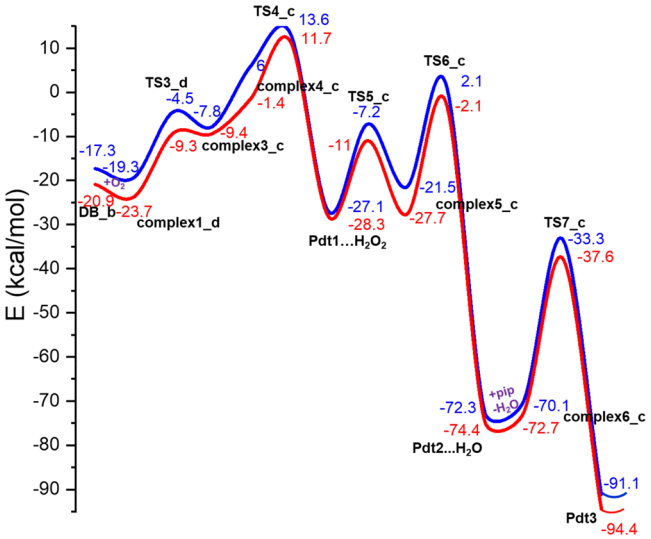

Figure 4. Electronic energy diagram for the formation of the addition product from C_{60} with piperidine dimer in the presence of O_2 in the gas phase (blue color) and pip solvent (red color).

the DB_b complex of C_{60}···$(pip)_2$ provides a different energy profile. The O_2 molecule binds with the same motif as in the previous case to outer piperidine, resulting in the complex1_d with significantly larger stability (19.3 and 23.7 kcal/mol in the gas phase and solvent, respectively) than upon binding of a single pip. Similar to the reaction scheme found for C_{60}···pip, the (NH) hydrogen atom transfers to $^3O_2$ and forms complex3_c in which the hydroperoxyl radical binds to the N atom of outer piperidine. An enhanced electrophilicity of the N atom in outer piperidine in the presence of O_2 explains this observation. The calculated local Fukui function value at the N atom of pip_2 is 0.01 and increases to 0.013 in the pip_2−O_2 complex (complex1_f). It assists the (NH) hydrogen transfer from inner to outer piperidine.

This reaction proceeds via the transition state TS3_d. Both structures, complex3_c and TS3_d, are stable, by 7.8 and 4.5 kcal/mol in the gas phase and by about 9.4 and 9.3 kcal/mol in the solvent, respectively, with respect to the isolated substrates.

From complex2_c, the formation of 1,4-diamino-C_{60} (Pdt1) requires additional pip in Scheme 3, while it binds the *outer* pip to C_{60} (complex3_c) in Scheme 4. The additional/outer piperidine molecule reacts with C_{60} through SN2″ pathway to form complex4_c. The reaction path prefers the 1,4-addition over the 1,2-addition of two pip to the hexagon systems, avoiding the steric hindrance in the complex. The hydroperoxyl radical abstracts the hydrogen in complex4_c through a transition state, TS4_c, to form diamionofullerene with hydrogen peroxide (Pdt1···H_2O_2). The stabilization of the Pdt1···H_2O_2 excludes the possibility of releasing the hydroperoxyl radical over hydrogen peroxide (Figures 3 and 4). The formation of 1,4-diamino-C_{60} epoxide (Pdt2) considers the same modifications. The highly electrophilic fulvene, Pdt1, goes through an epoxidation reaction with hydrogen peroxide. Pdt3 is formed from Pdt2 with additional pip. The direct attack of pip opens the epoxide ring forming a triamino hydroxyl product. In all these cases, the gas phase and the solvent calculation results are very similar, giving largely stabilized adduct products.

2.2. FT-IR Spectra. Figure 5 displays the IR spectra of the mixture of C_{60} with piperidine obtained immediately after the

https://doi.org/10.1021/jacs.1c01542
J. Am. Chem. Soc. 2021, 143, 10930−10939

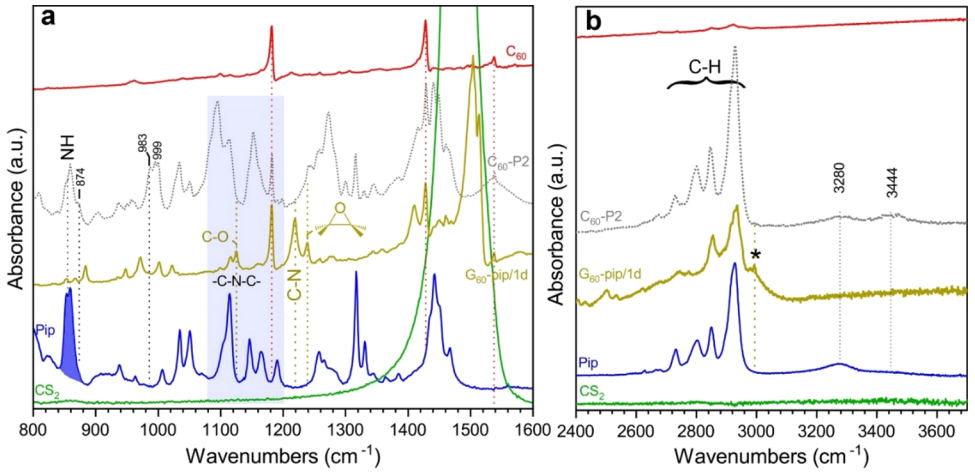

Figure 5. FT-IR spectra of the C_{60}–piperidine adduct after mixing in carbon disulfide (CS_2) for 1 day and after drying some of the solvent and possibly unbound piperidine molecules (C_{60} pip/1d). Spectra show the regions of (a) the C–N stretching and N–H bending and wagging vibrations and (b) the N–H stretching vibrations. The spectra of pure C_{60}, piperidine, CS_2, and the coordination complex of C_{60} with piperidine (C_{60}-P2, from ref 36) are given for comparison.

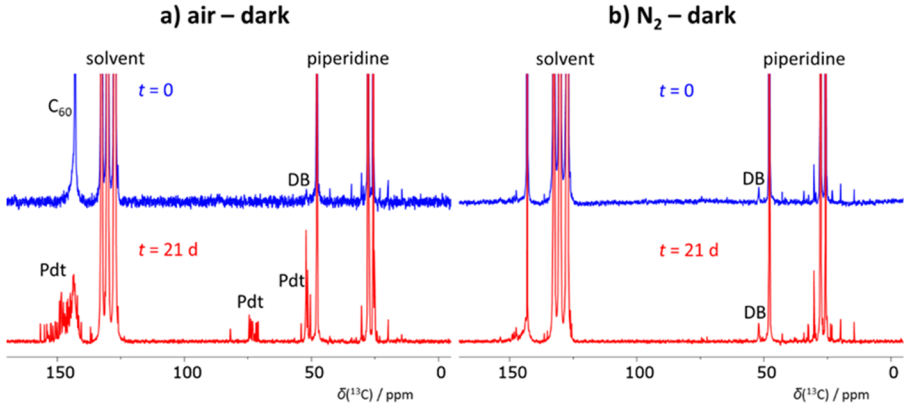

Figure 6. ^{13}C NMR spectra of the 1,2-dichlorobenzene-d_4 solutions of a mixture of C_{60} with piperidine. The samples were kept in the dark and under (a) ambient and (b) nitrogen atmospheres.

reaction starts to avoid a long exposure to air (taken from ref 36, spectrum C_{60}-P2 in Figure 5) and with a one-day delay (spectrum C_{60}–pip/1d in Figure 5). The latter lacks both the bands previously (ref 36) assigned to bending (Figure 5a) and stretching (Figure 5b) N–H vibrations. The loss of hydrogen from piperidine's N–H group is also visible from the dramatic intensity depletion of the N–H wagging vibration[40] of piperidine at ca. 855 cm^{-1} (Figure 5a). Furthermore, a new band appears slightly below 3000 cm^{-1} (Figure 5b), attributed to the new C–H bond on the fullerene's carbon. The strong covalent C–N between C_{60} and piperidine also emerged with significant intensity (indicated in Figure 5a) at ca. 1220 cm^{-1}. The above-described differences between the C_{60}-P2 and C_{60}–pip/1d spectra strongly indicate the formation of the addition product. The IR spectra displayed in Figure 5a indicate the existence of Pdt2 and Pdt3 adduct products. In particular, the band at 1125 cm^{-1} (Figure 5a) fits well within the typical C–O bond vibrations of tertiary alcohols, as in Pdt3;[41] the bands in the region of 1230–1280 cm^{-1} correspond to medium-strong C–O stretching vibrations of oxirane groups[42] formed in Pdt2.

2.3. NMR Spectroscopy. *2.3.1. C NMR.* Figures 6 and S13 display the C NMR spectra obtained in the nitrogen and oxygen atmospheres in dark conditions; the spectra in the light conditions are shown in Figure S14. The spectra acquired shortly after the sample preparation show, apart from the signal of the starting C_{60} at 143 ppm and of the piperidine signals, a low-intense signal at 52 ppm. This signal was previously assigned to the CH_2 groups of piperidine in the dative bond with C_{60}.[36]

In the nitrogen atmosphere, in both light and dark, the C_{60} signal at 143 ppm persists, and no new signals appear during the time course of the experiment, i.e., 21 days, showing its stability in the oxygen-free environment. On the contrary, the signal at 143 ppm completely disappears within 21 days, and new signals appear in the aromatic 140–155 ppm region in the spectra collected in the ambient atmosphere. Besides, new signals appear in the aliphatic regions at 70–82 ppm and close to 50 ppm. The latter corresponds to the piperidine fragments present in the reaction products. The isolated signal close to 82 ppm corresponds to an sp^3 carbon attached to an OH group, i.e., a product with a structure similar to Pdt3 (Figure S13). The signals in the region of 70–75 ppm correspond to fullerene sp^3 carbon atoms attached to piperidine nitrogen (found in all products of the reaction) and to sp^3 carbon atoms, which are involved in a three-membered oxirane ring (similarly as in Pdt2).

In general, all the chemical shifts' ranges of the newly appeared signals in the experiment performed in the ambient

https://doi.org/10.1021/jacs.1c01542
J. Am. Chem. Soc. 2021, 143, 10930–10939

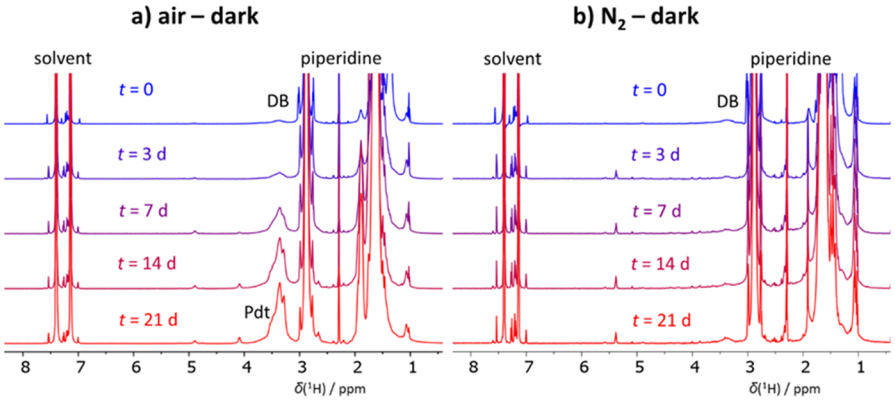

Figure 7. ^{1}H NMR spectra of the 1,2-dichlorobenzene-d_4 solutions of a mixture of C_{60} with piperidine. The samples were kept in the dark and under (a) an ambient atmosphere or (b) a nitrogen atmosphere.

Table 1. Interaction Energies (in kcal/mol) of C_{60} with pip and $(pip)_2$

				adduct formation					
	vdW	TS1	DB						
				TS2	Pdt				
C_{60}–pip	−5.6	−3.8	−9.3	+20.0	−12.9				
				C1	TS3	C2	Pdt1	Pdt2	Pdt3
C_{60}–pip + O_2	−5.6	−3.8	−9.3	−12.5	3.5	0.4	−22.3	−69.3	−101.0
				TS2	Pdt				
C_{60}–$(pip)_2$			−20.9	−5.4	−14.8				
				C1	TS3	C2	Pdt1	Pdt2	Pdt3
C_{60}–$(pip)_2$ + O_2			−20.9	−23.7	−9.3	−9.4	−15.7	−62.7	−94.4

atmosphere are close to those observed for piperidine addition to C_{60}.[29]

2.3.2. H NMR. The H NMR spectra (Figure 7) acquired immediately after the sample preparation in nitrogen and ambient atmospheres show a broad low-intense signal at 3.35 ppm. This signal was previously assigned to the CH_2 groups of piperidine in the dative bond with C_{60}[36] and proved the DB complex formation at the beginning of the reaction in both atmospheres. After 21 days, this signal changes only slightly in intensity in the nitrogen. Simultaneously, new signals with very low intensity appear in the regions of 3.5 and 5.5 ppm, indicating that some reaction occurs. The new signals are likely to originate from the interference of the 1,2-dichlorobenzene solvent, which might react either with traces of water or with piperidine. The possible product of these reactions is HCl, the presence of which (even traces) shifts the piperidine NH signals to higher chemical shifts.

The spectra of the samples kept in the ambient atmosphere give a more complex character, showing new signals at 3.2−4.2 ppm, which overlap with the original DB signal at 3.35 ppm. These new signals are assigned to the products of the addition reaction with the covalent bonds between C_{60} and piperidine. The NMR spectra of the samples kept in the light conditions are almost identical with those of the samples kept in the dark (see Figure S15).

2.4. Comparison of the Computational and Experimental Results. Table 1 collects the results of the reaction profile calculations given in Figures 1−4. Only the results performed in pip solvent are presented. Since the previous studies on the 5,6 and 6,6 fullerene adducts' relative energies (refs 37−39) and our results predict larger stabilities of the latter in all calculations, only these are used for the discussion. In our previous studies, we have predicted that the DB complex requires the hydrogen-bonded pip dimer to bind to C_{60}. This has been rationalized by the ΔG gas phase values of $C_{60}\cdots$pip (ΔG = 12.9 kcal/mol and ΔE = −2.5 kcal/mol; see Figure 1 and ref 36) and of $C_{60}\cdots(pip)_2$ (ΔG = −0.2 kcal/mol and ΔE = −17.3 kcal/mol; see Figure 2 and ref 36). The current results on the adduct formation support this prediction, giving lower energy barriers to the DB → adduct reaction in all investigated cases. Unlike in calculations performed for reactions in the presence of oxygen, the relative stabilities of DB and adduct Pdt complexes of $C_{60}\cdots(pip)_2$, obtained for calculations without O_2, predict the former to prevail in the reaction system. The larger stability of DB also follows from the Gibbs free energy calculations performed in the solvent environment, giving the ΔG values of −2.5 and −0.1 kcal/mol for the DB and Pdt, respectively. The calculated ΔG values of −43.2 kcal/mol (Pdt2) and −59.3 kcal/mol (Pdt3) also support the existence of stable adducts referred to in the literature.[29,33]

The results of FT-IR and NMR spectral measurements provide evidence of the dative bond formed at the very beginning of the complexation. Notably, the NMR spectra prove this complex's stability in the oxygen-free environment within the time course of several weeks. This observation agrees with computational predictions on the larger stability and, thus, a higher probability of the DB rather than the adduct complex existence.

Both FT-IR and NMR spectra further show that, with some time delay (1 day according to FT-IR results), the molecular oxygen shifts the reaction toward the addition reaction, previously investigated by several experimental groups (see the Introduction). New IR bands due to the C−H stretching modes slightly below 3000 cm^{-1} demonstrate the adduct formation. Note that the observed vibrational frequencies

https://doi.org/10.1021/jacs.1c01542
J. Am. Chem. Soc. 2021, 143, 10930−10939

nicely agree with the calculated C−H stretching frequencies of 2908 cm^{-1}. The adduct's formation in the air atmosphere is also confirmed by the intensive C−N stretching frequency observed at 1210 cm^{-1}, which is not detected in the DB complex.

Table 2 shows the results of the electronic properties of the $C_{60}\cdots(pip)_2$ complexes considered in the calculations. Notably,

Table 2. Properties of $C_{60}\cdots(pip)_2$ Complexes

	electron affinity[a]	charge transfer[b]	
	gas phase	gas phase	pip solvent
vdW	2.014	−0.160	
DB	1.575	−0.633	−0.683
Pdt(6,6)		−0.253	−0.263
Pdt1	2.121	0.203	0.218
Pdt2		0.661	0.724
Pdt3		0.559	0.550

[a]In eV. [b]Obtained from the NBO analyses.

although $C_{60}^{\bullet-}$ has not been identified in low-polar solvents in the previous studies (see the Introduction), our results of the natural-bond-orbital (NBO) analyses show relatively large electron transfer from pip to C_{60} in the DB complex. The charge transfer in adduct complexes is strikingly different, ranging from small pip → C_{60} electron transfer in Pdt(6,6) to the small transfer in the opposed direction in Pdt1, increasing significantly in Pdt2 and Pdt3, respectively. These differences are reflected in the ESP maps displayed in Figure S16. Importantly, for the redox potential characterizations, also, the values of electron affinities of the DB complex and adducts differ significantly. A comparison of the electron affinity (EA) of the vdW complex and pristine C_{60} (2.169 eV) gives almost an unchanged EA value of Pdt1, while that of DB decreases more significantly. These results indicate an extensive capability of functionalized C_{60} to provide systems with different characteristics by modifying only the surrounding environment.

3. CONCLUSION

The computational and experimental IR and NMR studies of the C_{60} complexes with the secondary amine piperidine have been performed to investigate their character under different reaction conditions. The studies conducted both in the oxygen-free environment and in the presence of O_2 reveal a different nature of the resulting products. The experimental studies prove that the dative bond complex forms at the beginning of the reaction course in all cases and remains stable in the oxygen-free atmosphere. On the basis of the kinetic and thermodynamic criteria obtained from the calculations, both dative bond and adduct formations proceed with pip2 rather than a single pip. The probability of DB and adduct existence differs for oxygen-free and oxygen atmospheres: in the former, the DB complex is more likely, while the calculations in the latter predict, in agreement with the previous and current experiments, the existence of the adduct products. The differences in the calculated electronic properties reflect a considerable versatility of C_{60}, and possibly other fullerenes, to modify their properties even by different conditions upon binding the same functional group. These observations reveal new opportunities for selective and straightforward covalent functionalization applicable to attractive fields, such as in energy storage (e.g., Li-ion batteries).

■ ASSOCIATED CONTENT

Supporting Information

The Supporting Information is available free of charge at https://pubs.acs.org/doi/10.1021/jacs.1c01542.

DFT results, computational details, and IR and NMR spectroscopy (PDF)

■ AUTHOR INFORMATION

Corresponding Authors

Pavel Hobza − *Institute of Organic Chemistry and Biochemistry, Czech Academy of Sciences, 16000 Prague, Czech Republic; IT4Innovations, VŠB-Technical University of Ostrava, 70800 Ostrava-Poruba, Czech Republic;* orcid.org/0000-0001-5292-6719; Email: pavel.hobza@uochb.cas.cz

Dana Nachtigallová − *Institute of Organic Chemistry and Biochemistry, Czech Academy of Sciences, 16000 Prague, Czech Republic; IT4Innovations, VŠB-Technical University of Ostrava, 70800 Ostrava-Poruba, Czech Republic;* orcid.org/0000-0002-9588-8625; Email: dana.nachtigallova@uochb.cas.cz

Authors

Rabindranath Lo − *Institute of Organic Chemistry and Biochemistry, Czech Academy of Sciences, 16000 Prague, Czech Republic; Regional Centre of Advanced Technologies and Materials, Czech Advanced Technology and Research Institute, Palacký University Olomouc, 77900 Olomouc, Czech Republic;* orcid.org/0000-0002-4436-3618

Debashree Manna − *Institute of Organic Chemistry and Biochemistry, Czech Academy of Sciences, 16000 Prague, Czech Republic*

Maximilián Lamanec − *Institute of Organic Chemistry and Biochemistry, Czech Academy of Sciences, 16000 Prague, Czech Republic; Department of Physical Chemistry, Palacký University Olomouc, 77146 Olomouc, Czech Republic; IT4Innovations, VŠB-Technical University of Ostrava, 70800 Ostrava-Poruba, Czech Republic*

Weizhou Wang − *College of Chemistry and Chemical Engineering and Henan Key Laboratory of Function-Oriented Porous Materials, Luoyang Normal University, Luoyang 471934, China;* orcid.org/0000-0002-4309-9077

Aristides Bakandritsos − *Regional Centre of Advanced Technologies and Materials, Czech Advanced Technology and Research Institute, Palacký University Olomouc, 77900 Olomouc, Czech Republic; Nanotechnology Centre, Centre of Energy and Environmental Technologies, VŠB-Technical University of Ostrava, 70800 Ostrava-Poruba, Czech Republic;* orcid.org/0000-0003-4411-9348

Martin Dračínský − *Institute of Organic Chemistry and Biochemistry, Czech Academy of Sciences, 16000 Prague, Czech Republic*

Radek Zbořil − *Institute of Organic Chemistry and Biochemistry, Czech Academy of Sciences, 16000 Prague, Czech Republic; Regional Centre of Advanced Technologies and Materials, Czech Advanced Technology and Research Institute, Palacký University Olomouc, 77900 Olomouc, Czech Republic; Nanotechnology Centre, Centre of Energy and Environmental Technologies, VŠB-Technical University*

https://doi.org/10.1021/jacs.1c01542
J. Am. Chem. Soc. 2021, 143, 10930−10939

of Ostrava, 70800 Ostrava-Poruba, Czech Republic;
orcid.org/0000-0002-3147-2196

Complete contact information is available at:
https://pubs.acs.org/10.1021/jacs.1c01542

Author Contributions

[‖]R.L., D.M., and M.L. contributed equally and are co-first authors.

Notes

The authors declare no competing financial interest.

■ ACKNOWLEDGMENTS

This work was supported by the Czech Science Foundation, the project 19-27454X (P.H., D.N., R.Z.) and the project 20-01472S (M.D.); by Palacký University, the Internal grant association, the project IGA_PrF_2021_031 (M.L.); by the ERDF/ESF project "Nano4Future" (No. CZ.02.1.01/0.0/0.0/16_019/0000754) (R.L., A.B.). W.W. gratefully acknowledges the National Science Foundation of China (21773104) for funding. We thank Tomáš Steklý for contributing to the sample preparation and the collection of IR spectra.

■ REFERENCES

(1) Garrido, M.; Gualandi, L.; Di Noja, S.; Filippini, G.; Bosi, S.; Prato, M. Synthesis and Applications of Amino-Functionalized Carbon Nano-materials. *Chem. Commun.* **2020**, *56* (84), 12698−12716.
(2) Maeda-Mamiya, R.; Noiri, E.; Isobe, H.; Nakanishi, W.; Okamoto, K.; Doi, K.; Sugaya, T.; Izumi, T.; Homma, T.; Nakamura, E. In Vivo Gene Delivery by Cationic Tetraamino Fullerene. *Proc. Natl. Acad. Sci. U. S. A.* **2010**, *107* (12), 5339−5344.
(3) Nakamura, E.; Isobe, H. In Vitro and in Vivo Gene Delivery with Tailor-Designed Aminofullerenes. *Chem. Rec.* **2010**, *10* (5), 260−270.
(4) Pantarotto, D.; Bianco, A.; Pellarini, F.; Tossi, A.; Giangaspero, A.; Zelezetsky, I.; Briand, J. P.; Prato, M. Solid-Phase Synthesis of Fullerene-Peptides. *J. Am. Chem. Soc.* **2002**, *124* (42), 12543−12549.
(5) Bosi, S.; Feruglio, L.; Da Ros, T.; Spalluto, G.; Gregoretti, B.; Terdoslavich, M.; Decorti, G.; Passamonti, S.; Moro, S.; Prato, M. Hemolytic Effects of Water-Soluble Fullerene Derivatives. *J. Med. Chem.* **2004**, *47* (27), 6711−6715.
(6) Friedman, S. H.; DeCamp, D. L.; Kenyon, G. L.; Sijbesma, R. P.; Srdanov, G.; Wudl, F. Inhibition of the HIV-1 Protease by Fullerene Derivatives: Model Building Studies and Experimental Verification. *J. Am. Chem. Soc.* **1993**, *115* (15), 6506−6509.
(7) Pastorin, G.; Marchesan, S.; Hoebeke, J.; Da Ros, T.; Ehret-Sabatier, L.; Briand, J. P.; Prato, M.; Bianco, A. Design and Activity of Cationic Fullerene Derivatives as Inhibitors of Acetylcholinesterase. *Org. Biomol. Chem.* **2006**, *4* (13), 2556−2562.
(8) Nakamura, E.; Isobe, H.; Tomita, N.; Sawamura, M.; Jinno, S.; Okayama, H. Functionalized Fullerene as an Artificial Vector for Transfection. *Angew. Chem., Int. Ed.* **2000**, *39* (23), 4254−4257.
(9) Klumpp, C.; Lacerda, L.; Chaloin, O.; Da Ros, T.; Kostarelos, K.; Prato, M.; Bianco, A. Multifunctionalised Cationic Fullerene Adducts for Gene Transfer: Design, Synthesis and DNA Complexation. *Chem. Commun.* **2007**, No. 36, 3762−3764.
(10) Jariwala, D.; Sangwan, V. K.; Lauhon, L. J.; Marks, T. J.; Hersam, M. C. Carbon Nanomaterials for Electronics, Optoelectronics, Photovoltaics, and Sensing. *Chem. Soc. Rev.* **2013**, *42* (7), 2824−2860.
(11) Collavini, S.; Delgado, J. L. Fullerenes: The Stars of Photovoltaics. *Sustainable Energy and Fuels.* **2018**, *2*, 2480−2493.
(12) Fernández, G.; Sánchez, L.; Veldman, D.; Wienk, M. M.; Atienza, C.; Guldi, D. M.; Janssen, R. A. J.; Martín, N. Tetrafullerene Conjugates for All-Organic Photovoltaics. *J. Org. Chem.* **2008**, *73* (8), 3189−3196.
(13) Mateo-Alonso, A.; Ehli, C.; Rahman, G. M. A.; Guldi, D. M.; Fioravanti, G.; Marcaccio, M.; Paolucci, F.; Prato, M. Tuning Electron Transfer through Translational Motion in Molecular Shuttles. *Angew. Chem., Int. Ed.* **2007**, *46* (19), 3521−3525.
(14) Campisciano, V.; Gruttadauria, M.; Giacalone, F. Modified Nanocarbons for Catalysis. *ChemCatChem* **2019**, *11* (1), 90−133.
(15) López-Andarias, J.; Frontera, A.; Matile, S. Anion-π Catalysis on Fullerenes. *J. Am. Chem. Soc.* **2017**, *139* (38), 13296−13299.
(16) Rosso, C.; Emma, M. G.; Martinelli, A.; Lombardo, M.; Quintavalla, A.; Trombini, C.; Syrgiannis, Z.; Prato, M. A Recyclable Chiral 2-(Triphenylmethyl)Pyrrolidine Organocatalyst Anchored to [60]Fullerene. *Adv. Synth. Catal.* **2019**, *361* (12), 2936−2944.
(17) Jiang, Z.; Zhao, Y.; Lu, X.; Xie, J. Fullerenes for Rechargeable Battery Applications: Recent Developments and Future Perspectives. *J. Energy Chem.* **2021**, *55*, 70−79.
(18) Sood, P.; Kim, K. C.; Jang, S. S. Electrochemical and Electronic Properties of Nitrogen Doped Fullerene and Its Derivatives for Lithium-Ion Battery Applications. *J. Energy Chem.* **2018**, *27* (2), 528−534.
(19) Teprovich, J. A.; Weeks, J. A.; Ward, P. A.; Tinkey, S. C.; Huang, C.; Zhou, J.; Zidan, R.; Jena, P. Hydrogenated C_{60} as High-Capacity Stable Anode Materials for Li Ion Batteries. *ACS Appl. Energy Mater.* **2019**, *2* (9), 6453−6460.
(20) Jiang, Z.; Zeng, Z.; Yang, C.; Han, Z.; Hu, W.; Lu, J.; Xie, J. Nitrofullerene, a C_{60}-Based Bifunctional Additive with Smoothing and Protecting Effects for Stable Lithium Metal Anode. *Nano Lett.* **2019**, *19* (12), 8780−8786.
(21) Shan, C.; Yen, H. J.; Wu, K.; Lin, Q.; Zhou, M.; Guo, X.; Wu, D.; Zhang, H.; Wu, G.; Wang, H. L. Functionalized Fullerenes for Highly Efficient Lithium Ion Storage: Structure-Property-Performance Correlation with Energy Implications. *Nano Energy* **2017**, *40*, 327−335.
(22) Hirsch, A.; Li, Q.; Wudl, F. Globe-trotting Hydrogens on the Surface of the Fullerene Compound $C_{60}H_6(N(CH_2CH_2)_2O)_6$. *Angew. Chem., Int. Ed. Engl.* **1991**, *30* (10), 1309−1310.
(23) Wudl, F.; Hirsch, A.; Khemani, K. C.; Suzuki, T.; Allemand, P.-M.; Koch, A.; Eckert, H.; Srdanov, G.; Webb, H. M. Survey of Chemical Reactivity of C_{60}, Electrophile and Dieno−Polarophile Par Excellence. In *Fullerenes*; American Chemical Society, 1992; pp 161−175.
(24) Schick, G.; Kampe, K. D.; Hirsch, A. Reaction of [60]Fullerene with Morpholine and Piperidine: Preferred 1,4-Additions and Fullerene Dimer Formation. *J. Chem. Soc., Chem. Commun.* **1995**, No. 19, 2023−2024.
(25) Hirsch, A. Addition Reactions of Buckminsterfullerene (C60). *Synthesis* **1995**, *1995*, 895−913.
(26) Kampe, K.-D.; Egger, N.; Vogel, M. Diamino and Tetraamino Derivatives of Buckminsterfullerene C_{60}. *Angew. Chem., Int. Ed. Engl.* **1993**, *32* (8), 1174−1176.
(27) Isobe, H.; Ohbayashi, A.; Sawamura, M.; Nakamura, E. A Cage with Fullerene End Caps. *J. Am. Chem. Soc.* **2000**, *122*, 2669−2670.
(28) Isobe, H.; Tomita, N.; Nakamura, E. One-Step Multiple Addition of Amine to [60]Fullerene. Synthesis of Tetra(Amino)-Fullerene Epoxide under Photochemical Aerobic Conditions. *Org. Lett.* **2000**, *2* (23), 3663−3665.
(29) Li, Y.; Gan, L. Selective Addition of Secondary Amines to C_{60}: Formation of Pentaand Hexaamino[60]Fullerenes. *J. Org. Chem.* **2014**, *79* (18), 8912−8916.
(30) Skiebe, A.; Hirsch, A.; Klos, H.; Gotschy, B. $[DBU]C_{60}$. Spin Pairing in a Fullerene Salt. *Chem. Phys. Lett.* **1994**, *220* (1−2), 138−140.
(31) Klos, H.; Rystau, I.; Schütz, W.; Gotschy, B.; Skiebe, A.; Hirsch, A. Doping of C_{60} with Tertiary Amines: TDAE, DBU, DBN. A Comparative Study. *Chem. Phys. Lett.* **1994**, *224* (3−4), 333−337.
(32) Fujitsuka, M.; Luo, C.; Ito, O. Electron-Transfer Reactions between Fullerenes (C_{60} and C_{70}) and Tetrakis(Dimethylamino)-Ethylene in the Ground and Excited States. *J. Phys. Chem. B* **1999**, *103* (3), 445−449.

(33) Isobe, H.; Tanaka, T.; Nakanishi, W.; Lemiègre, L.; Nakamura, E. Regioselective Oxygenative Tetraamination of [60]Fullerene. Fullerene-Mediated Reduction of Molecular Oxygen by Amine via Ground State Single Electron Transfer in Dimethyl Sulfoxide. *J. Org. Chem.* **2005**, *70* (12), 4826−4832.
(34) Sun, Y.-P.; Ma, B.; Bunker, C. E. Photoinduced Intramolecular n−π^* Electron Transfer in Aminofullerene Derivatives. *J. Phys. Chem. A* **1998**, *102* (39), 7580−7590.
(35) Wang, N. X. Photochemical Addition Reactions of [60]-Fullerene with 1,2-Ethylenediamine and Piperazine. *Tetrahedron* **2002**, *58* (12), 2377−2380.
(36) Lamanec, M.; Lo, R.; Nachtigallová, D.; Bakandritsos, A.; Mohammadi, E.; Dračínský, M.; Zbořil, R.; Hobza, P.; Wang, W. The Existence of a N→C Dative Bond in the C_{60}−Piperidine Complex. *Angew. Chem., Int. Ed.* **2021**, *60*, 1942−1950.
(37) Basiuk, E. V.; Basiuk, V. A.; Shabel'nikov, V. P.; Golovatyi, V. G.; Ocotlán Flores, J.; Saniger, J. M. Reaction of Silica-Supported Fullerene C_{60} with Nonylamine Vapor. *Carbon* **2003**, *41* (12), 2339−2346.
(38) Ramírez-Calera, I. J.; Meza-Laguna, V.; Gromovoy, T. Y.; Chávez-Uribe, M. I.; Basiuk, V. A.; Basiuk, E. V. Solvent-Free Functionalization of Fullerene C_{60} and Pristine Multi-Walled Carbon Nanotubes with Aromatic Amines. *Appl. Surf. Sci.* **2015**, *328*, 45−62.
(39) Thong, N. M.; Vo, Q. V.; Le Huyen, T.; Van Bay, M.; Dung, N. N.; Thu Thao, P. T.; Nam, P. C. Functionalization and Antioxidant Activity of Polyaniline-Fullerene Hybrid Nanomaterials: A Theoretical Investigation. *RSC Adv.* **2020**, *10* (25), 14595−14605.
(40) *The Handbook of Infrared and Raman Characteristic Frequencies of Organic Molecules*; Elsevier Inc., 1991; https://www.sciencedirect.com/book/9780124511606/the-handbook-of-infrared-and-raman-characteristic-frequencies-of-organic-molecules (accessed Jan 14, 2021).
(41) Socrates, G. *Infrared and Raman Characteristic Group Frequencies: Tables and Charts*, 3rd ed.; John Wiley & Sons Ltd.: Chichester, England, 2001; p 94.
(42) Socrates, G. *Infrared and Raman Characteristic Group Frequencies: Tables and Charts*, 3rd ed.; John Wiley & Sons Ltd.: Chichester, England, 2001; p 102.

https://doi.org/10.1021/jacs.1c01542
J. Am. Chem. Soc. 2021, 143, 10930−10939